Cardiac Na Currents and the Inactivating, Reopening, and Waiting Properties of Single Cardiac Na Channels

D. L. KUNZE, A. E. LACERDA, D. L. WILSON, and A. M. BROWN

From the Department of Physiology and Biophysics, University of Texas Medical Branch, Galveston, Texas 77550

ABSTRACT Tetrodotoxin (TTX)-sensitive Na currents were examined in single dissociated ventricular myocytes from neonatal rats. Single channel and whole cell currents were measured using the patch-clamp method. The channel density was calculated as $2/\mu m^2$, which agreed with our usual finding of four channels per membrane patch. At 20°C, the single channel conductance was 20 pS. The open time distributions were fit by a single-exponential function with a mean open time of ~1.0 ms at membrane potentials from −60 to −40 mV. Averaged single channel and whole cell currents were similar when scaled and showed both fast and slow rates of inactivation. The inactivation and activation gating shifted quickly to hyperpolarized potentials for channels in cell-attached as well as excised patches, whereas a much slower shift occurred in whole cells. Slowly inactivating currents were present in both whole cell and single channel current measurements at potentials as positive as −40 mV. In whole cell measurements, the potential range could be extended, and slow inactivation was present at potentials as positive as −10 mV. The curves relating steady state activation and inactivation to membrane potential had very little overlap, and slow inactivation occurred at potentials that were positive to the overlap. Slow inactivation is in this way distinguishable from the overlap or window current, and the slowly inactivating current may contribute to the plateau of the rat cardiac action potential. On rare occasions, a second set of Na channels having a smaller unit conductance and briefer duration was observed. However, a separate set of threshold channels, as described by Gilly and Armstrong (1984. *Nature* [*Lond.*]. 309:448), was not found. For the commonly observed Na channels, the number of openings in some samples far exceeded the number of channels per patch and the latencies to first opening or waiting times were not sufficiently dispersed to account for the slowly inactivating currents; the slow inactivation was produced by channel reopening. A general model was developed to predict the number of openings in each sample. Models in which the number of openings per sample was due to a dispersion of waiting times combined with a rapid transition from an open to

Address reprint requests to Dr. Diana L. Kunze, Dept. of Physiology and Molecular Biophysics, Baylor College of Medicine, Houston, TX 77030.

an absorbing inactivated state were unsatisfactory and a model that was more consistent with the results was identified.

INTRODUCTION

Differences presently exist regarding the inactivation of cardiac Na currents. In syncytial preparations such as rabbit cardiac Purkinje fibers and cultured cardiac myoballs, inactivation has been described as monoexponential (Colatsky, 1980; Ebihara and Johnson, 1980), in agreement with the original description for squid axon (Hodgkin and Huxley, 1952). However, a slower component of inactivation has been identified in canine cardiac Purkinje fibers (Gintant et al., 1984). In ventricular cells, specifically single rat ventricular myocytes, fast and slow phases of inactivation having time constants with a ratio of ~0.1 were first described by Brown et al. (1981*b*) and confirmed by Zilberter et al. (1982); Bodewei et al. (1982), however, described only the fast phase. The problem is important because a persistent Na current may contribute to the plateau of the cardiac action potential and the refractory period. In fact, evidence in support of the first possibility comes from a number of experiments that have shown that tetrodotoxin (TTX) shortens the cardiac action potential (Dudel et al., 1967; Corabouef et al., 1979). The latter result is not conclusive, however, since it could be reconciled with a single inactivation process by attributing the effect to a window current that arises from overlap between the potential dependence of inactivation and activation (Attwell et al., 1979).

There are several possible explanations for the slower inactivation process. One is that cardiac Na channels have two inactivated states, as proposed by Brown et al. (1981*b*). A second is that a completely different set of Na channels is involved. Support for this idea comes from the demonstration of more than two types of Na channel in mouse neuroblastoma cells (Nagy et al., 1983), a report of differential sensitivity to TTX of single cardiac Na channels (Ten Eick et al., 1984), and a note on a separable threshold Na current in squid axon (Gilly and Armstrong, 1984). A variation of this idea is the proposal by Patlak and Ortiz (1985) that a single set of Na channels can have two modes of behavior, one of which causes the slow inactivation. Whatever the mechanism, attention must also be paid to the new concept of Na channel kinetics suggested by Aldrich et al. (1983) and Aldrich and Stevens (1984). From studies on single Na channels in neuroblastoma and GH4 cells, Aldrich and co-workers have observed that latencies to first opening or waiting times are dispersed widely in time and that channels tend to open only once during a depolarizing step. Contrary to presently held ideas that activation is fast and inactivation is relatively slower, they have proposed that activation is slow and inactivation is both fast and essentially final; there is one inactivated state and it is absorbing. We shall refer to this as the ACS (Aldrich, Corey, Stevens) model. The ACS model has been evaluated by Horn and Vandenberg (1984) in GH3 cells and they have found quantitative discrepancies that led them to suggest a more complete version. In the experiments described here, we have tried to provide answers to some of the questions we have raised concerning cardiac Na channels. We have confirmed the occurrence of slow inactivation in neonatal rat cardiac myocytes, shown that it is a

property of the most frequently found set of single cardiac Na channels, and excluded certain models as explanations.

METHODS

Preparation

Hearts were removed from 8–12 neonatal rats and placed together in Dulbecco's modified Eagle's medium supplemented with 10% fetal calf serum (DMEM-10FCS; Mark and Strasser, 1966). Atria and surrounding tissue were cut away from ventricles in nominally Ca^{2+}- and Mg^{2+}-free Hanks' solution. Each ventricle was cut into 7–10 pieces and placed in 5 ml of 0.5% trypsin in Hanks' solution and digested for 5 min at 37°C. This digestion was repeated twice and supernatants from the second and third digestion were collected in a 50-ml centrifuge tube containing 0.5 ml DMEM-10FCS to stop enzyme action. Cells were pelleted, the supernatant was discarded, and the cells were resuspended, plated, and cultured in DMEM-10FCS. Cells were commonly used within 24–48 h.

Electrophysiological Measurements

Cell-attached gigaseals were obtained using fire-polished Pyrex micropipettes of 1–10 MΩ resistance (Hamill et al., 1981). To reduce the capacity transient, Sylgard was applied as close to the pipette tip as possible. For cell-attached single channel recording, the pipette contained (mM): 137 NaCl, 5.4 KCl, 1 $MgCl_2$, 2 or 0.02 $CaCl_2$, 10 glucose, 10 HEPES (pH 7.3). This was also used for the extracellular solution. Because of the uncertainty of the actual resting potentials during the lengthy recordings, in several experiments the cells were depolarized to ~0 mV using a bathing solution containing 150 mM KCl, 10 mM HEPES, pH 7.4.

The patch clamp used for whole cell recording measures membrane potential directly and was designed and constructed by Dr. T. Iwazumi of our department. It incorporates several new circuit design and construction methods to provide high bandwidth and low noise. The design features of this clamp will be described in a forthcoming publication (Lacerda, A. E., T. Iwazumi, and A. M. Brown, manuscript in preparation). After the formation of a cell-attached patch, the cell membrane in the pipette was ruptured as described in Hamill et al. (1981). Transient cancellation, clamp gain, bandwidth, and series resistance adjustments were made to provide optimum settling and attenuation of the capacitive current transient. Most whole cell data were obtained from spherical cells cultured for 1–2 d. For whole cell recording, the patch pipette contained a solution with the following composition (mM): 120 CsCl, 1 $CaCl_2$, 11 EGTA, 2 $MgCl_2$, 10 glucose, 10 HEPES (pH 7.2). The extracellular solution composition was (mM): 100 NaCl, 5.4 KCl, 2 $MgCl_2$, 0.020 $CaCl_2$, 20 CsCl, 20 TEA, 5 4-aminopyridine (4-AP), 10 glucose, 10 HEPES (pH 7.4). A low-Na bath solution had the following composition (mM): 40 NaCl, 55 *N*-methyl-D-glucamine (NMDG), 5.4 KCl, 2 $MgCl_2$, 0.020 $CaCl_2$, 20 CsCl, 30 TEA, 5 4-AP, 20 glucose, 10 HEPES (pH 7.4). All experiments were done at room temperature (20°C). Exceptions to these conditions are noted in the text.

To detect the presence of threshold currents, we used either a brief, weakly activating pulse from various holding potentials or a single holding potential combined with a similar activating step and a variety of return potentials. Steady state parameters for $h_\infty(v)$ were determined with the usual conditioning test-pulse protocols. The prepulse duration was 600 ms and the test pulse was −10 mV. The activation of the Na system was measured either from the magnitudes of the current tails at the end of brief activating pulses of different amplitudes or from the fit to the turn-on of Na currents during a pulse using a Hodgkin and Huxley (H-H) m^3h model. The data have not been corrected for liquid junction potentials that were $<4.4 \pm 3$ mV.

Data Acquisition and Analysis

The single channel data were analog-filtered before digitization using a four-pole Bessel filter and a cut-off frequency of 5–10 kHz. The sampling rate always exceeded the Nyquist rate. The data were corrected for leakage and remaining capacity transients by summing and averaging traces with no activity (nulls or failures) and subtracting the average from each trace with activity. The data were then digitally filtered using a zero-phase, four-pole filter (Brown et al., 1984) at a high-frequency cut-off of 1–2 kHz. The transitions between closed and open states were determined using an automated threshold detection scheme (Lux and Brown, 1984) in which threshold was set at three to four times the standard deviation of the background current noise. This level was usually about half the maximum amplitude (HMA) of unitary events. Points above threshold in the 5–10-kHz data were averaged and the HMAs in the 1–2-kHz data were redetermined to give a new threshold. The process was iterated until the two points defining the HMAs were no longer changing. From these measurements, idealized rectangular unitary events were established. The process for detecting the amplitude was iterated in order to detect and idealize overlapping openings. In the latter case, errors may occur when there is 50% overlap and the program allows the user to correct the idealized trace. The idealized events were the basis for the histograms we used. Waiting, closed, and open time distributions were fit to sum-of-exponentials probability density functions using the method of maximum likelihood as described by Colquhoun and Sigworth (1983). Maximization of the likelihood function was achieved using a modified Marquardt algorithm. Parameter standard deviations were obtained via a method suggested by Colquhoun and Sigworth (1983). The open times of overlapping events were arbitrarily assigned as follows. For the case of two events, the assignations were one long and one short time rather than two more intermediate values. For three events, the assignations were one long, one short, and one intermediate. This process biases the distribution of open times but does not change the mean values (Fenwick et al., 1982). The mean values minus the threshold-detection-system dead time were comparable to the maximum-likelihood estimates (Colquhoun and Sigworth, 1983). Our program also produced plots of the distributions of the number of openings per trace. These distributions were fit to the model described later using a maximum-likelihood technique. In this case, the simplex method (Nelder and Mead, 1965) was used for maximization. In the parameter-estimation programs, constraints could be placed on parameters using a transformation of the variables method (Bard, 1974); e.g., the probability parameters described later were limited to values between 0 and 1.

Whole cell currents were recorded after analog filtering to 10 or 20 kHz and digitized at rates as fast as 2 μs/point using a 12-bit signal averager (Nicolet Instrument Corp., Madison, WI). Linear components of leakage and capacitance were subtracted using appropriately scaled hyperpolarizing pulses. Currents were fitted using the Marquardt method to models such as a sum of exponentials, the H-H model, and a modified H-H model with biexponential inactivation.

Relating the Number of Openings Measured per Sample to Model Parameters

We analyzed in considerable detail the measurements of the number of openings per record. Such measurements were described in terms of the following general relation for the probability of a channel having j openings in a record (Appendix A):

$$P(j) = [1 - P(0)](1 - \rho)\rho^{j-1}, \qquad j = 0, 1, \ldots \tag{1}$$

In this equation, there are two unknown parameters, $P(0)$ and ρ, where $P(0)$ is the probability of zero openings, and ρ is equal to the probability that a channel reopens (see

Appendix A). In Appendix A, some simple state models, such as model M_1, which includes the ACS model, were analyzed in terms of their predictions for $P(j)$, and the equations in Table III and Eq. A7 relate the model parameters to ρ and $P(0)$. Thus, one can obtain ρ and $P(0)$ from measurements as described below and then compute various model parameters. An additional theoretical result in Appendix B allows for the correction of missed fast openings. This is done by deriving an apparent probability distribution, called $P_A(j)$.

The first method for obtaining ρ and $P(0)$ consisted of fitting the frequency distributions of the number of openings in a trace. In this case, the measured distributions were fitted with the apparent probability distribution, $P_A(j)$, given in Eqs. B7 and B8. For the case of N independent identical channels, this distribution was numerically convolved with itself N times, giving

$$_NP_A(j) = [P_A(j)]^{N*}, \tag{2}$$

where the superscript $N*$ indicates an N-fold convolution after the notation of ACS. Referring to Eqs. B7, B8, and 1, P_D was computed as described in Appendix B, and ρ and $P(0)$ were free parameters when Eq. 2 was fitted to the data.

Values for ρ and $P(0)$ were also obtained from average quantities using the following results. From Eq. 2, it was found that $_NP_A(0)$ is given by the Nth power of $P_A(0)$. Thus,

$$P_A(0) = [_NP_A(0)]^{1/N}. \tag{3}$$

From Eq. B8, $P(0)$ can be obtained from

$$P(0) = \frac{P_A(0) - G}{1 - G}, \tag{4}$$

where

$$G = \frac{(1 - \rho)(1 - P_D)}{1 - \rho + \rho P_D}. \tag{5}$$

In the case of N channels, the average number of apparent openings, $_N\bar{j}_A$, is N times the result for one channel. Thus,

$$\bar{j}_A = {}_N\bar{j}_A/N. \tag{6}$$

Substituting Eqs. 4 and 5 into Eq. B9, and substituting from Eqs. A3 and A4 and rearranging, one obtains

$$\rho = \frac{\bar{j}_A + P_A(0) - 1}{\bar{j}_A + [P_A(0) - 1](1 - P_D)}. \tag{7}$$

Thus, $_N\bar{j}_A$ and $_NP_A(0)$ were measured, $\bar{j}_A$ and $P_A(0)$ were calculated from Eqs. 3 and 6, and ρ and $P(0)$ were calculated from Eqs. 4, 5, and 7. In turn, other quantities of interest were calculated from ρ and $P(0)$.

RESULTS

We deliberately chose to do our experiments on neonatal myocytes (neocytes) rather than adult rat ventricular myocytes because neocytes have been used successfully for single channel recording, including single Na channels (Cachelin et al., 1983), and because their spheroidal shape and the absence of T-tubules make them particularly suitable for the single-electrode gigaseal method of voltage-clamping the whole cell (Lacerda et al., manuscript in preparation; Figs.

5, 6, and 11–14). Whole cell clamping was used because evaluation of slow inactivation required test potentials at which the resolution of the single channel method becomes limiting. By using the same preparation, we could compare whole cell and single channel measurements over a restricted potential range and then make more valid extrapolations from the single channel data over a wider range of potentials. The advantage of neocytes over adult myocytes is that

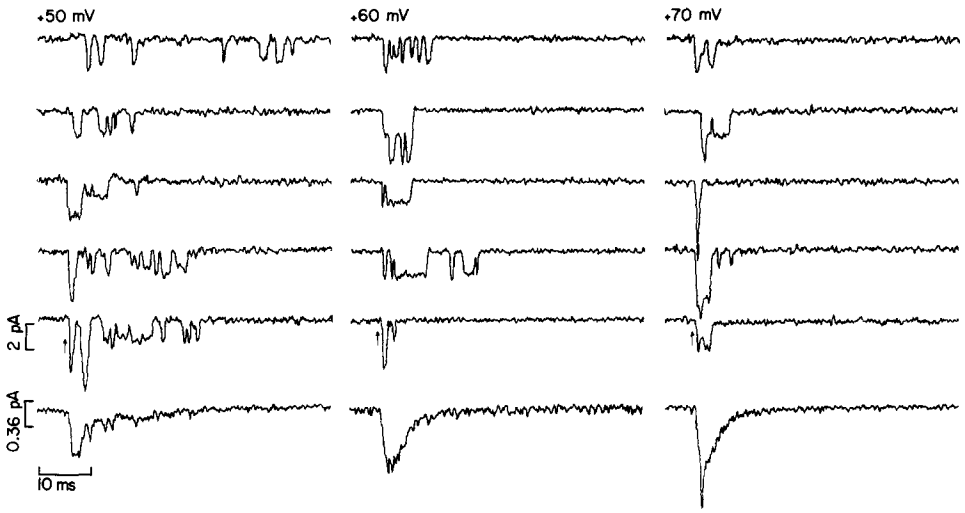

FIGURE 1. Single Na channel activity. (Top) Samples of records of single Na channel activity from a cell-attached patch on a neonatal rat ventricular myocyte. The holding potential was −60 mV relative to the resting potential, V_R. h_∞ is ~0.85 (see Fig. 5). Step depolarizations were delivered every 4 s and were 60 ms in duration and either 50, 60, or 70 mV in amplitude. The data were initially filtered to 5 kHz using an eight-pole Bessel filter and sampled at 20 kHz. Subsequently, the data were filtered to 1.2 kHz using a zero-phase digital filter. The linear components of resistance and capacitance were subtracted using samples that contained no events (nulls or failures). The arrow indicates the onset of the pulse. The fraction of failures at each potential was 7, 4, and 3% at +50, +60, and +70 mV, respectively. Note the large number of openings per sample, especially for the 50- and 60-mV steps. Simultaneous openings of three units are shown at the 70-mV step. In some records not shown in this figure, four simultaneous openings were observed and the number of channels in the patch was estimated as four using a maximum-likelihood estimator (see text). (Bottom) Single channel records (including the failures) at each potential were summed and averaged, and are displayed below the samples of the single channel records.

for the measurement of whole cell Na currents, the complex geometry of the latter requires the use of the more demanding hybrid suction pipette method of internal perfusion and voltage clamp (Brown et al., 1981*a*).

Evaluation of the Number of Openings per Sample

Some representative records or samples from a cell-attached patch on a neocyte are shown in Fig. 1. 995 samples were taken from this patch. The illustrated

records were made using a patch holding potential that was 60 mV hyperpolarized from the resting potential, V_R, and depolarizing steps that were 50, 60, and 70 mV in amplitude. At the largest steps, simultaneous openings of four times the unitary amplitude occurred soon after the depolarizing step, which indicated that N, the number of Na channels in the patch, was at least 4. A nonstationary maximum-likelihood estimation of N (Patlak and Horn, 1982) also gave a probable value of 4. The peak values for P_o using an N of 4 were 0.09, 0.13, and 0.20, respectively, at the three test potentials referred to. Assuming a resting potential of −50 mV, these values agree favorably with the $m_\infty(v)$ curve of whole cell currents shown in Fig. 13. Fig. 1 also shows that the summed single channel currents rose to a peak (or activated) and then subsided more slowly (or inactivated), with the rates of each process increasing as the step amplitudes were increased. The waveforms compare favorably with the whole cell current waveforms recorded at the same potentials as shown in Figs. 12 and 14. This is discussed in more detail later. The relation between the appearance of openings and holding potential was associated with a very steep potential dependence of peak opening probability and latency to first opening or waiting time. The latter, along with N's of at least 2 and usually 4 per patch, caused the sudden appearance of simultaneous openings at the onset of the voltage step as the step amplitudes were progressively increased above threshold. Channel openings with these characteristics were absent when the patch pipette contained TTX (5×10^{-5} M) or when the membrane patch was held at potentials <20 mV hyperpolarized from the cell's resting potential. Therefore, we are confident that the channels being recorded were Na channels.

The occurrence of many openings in each record or sample was a noticeable feature that was particularly striking when compared with the published records of Aldrich et al. (1983). On the other hand, the published records of Fukushima (1981), Fenwick et al. (1982), Cachelin et al. (1983), Nagy et al. (1983), Ten Eick et al. (1984), and Horn et al. (1984) show numerous openings per sample. In the present experiments, the number of openings was sometimes 12 per sample and occasionally 20 per sample and was much greater than the N of 4 for this patch.

Fig. 2 shows 10 frequency distributions of the number of openings in a trace from a membrane patch that gave 995 traces. These were obtained with various combinations of holding and test potentials. The data were fitted with the discrete probability distribution for apparent openings, ${}_NP_A(j)$ (Eq. 2), which was based on a general equation for openings per sample (Appendix A) and which was corrected for missed openings (Appendix B). In these fits, the number of channels was estimated as described in the Methods, and P_R ($t = 0$), the fraction of channels in the rested state available for a subsequent activation (h_∞ in Hodgkin-Huxley notation), was estimated using the usual conditioning test-pulse protocol shown in Fig. 5. The fits of the theory to the data were fairly good. As shown in Fig. 3, the fits of ${}_NP_A(j)$ to the measured distributions was better than the fit of model M_1 (see Appendix A and Table III) or the fit of the general equation assuming no fast openings to be missed.

The parameter estimates for $P(0)$ and ρ obtained by fitting the distributions are given in Table I. The ρ and $P(0)$ values obtained at a test potential were

fairly consistent for a given patch as long as the holding potential was more negative than $V_R - 60$ (compare ID numbers 604, 702, and 500). Values tended to vary between different patches. As a function of depolarizing test potential, $P(0)$ tended to increase and ρ tended to decrease. The calculated values for

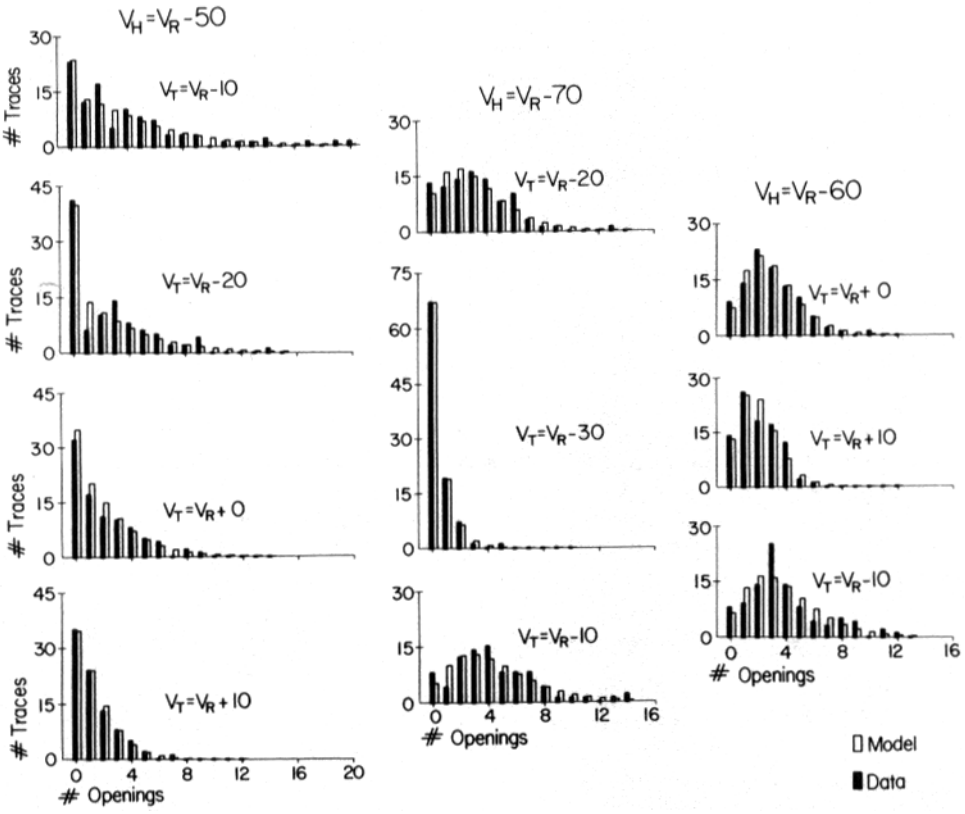

FIGURE 2. Frequency distributions of number of openings per record. The filled bars are the number of openings per trace for various combinations of holding potential and test potential and the open bars are the predictions from the generalized model, M_3 (see text). The histograms are displayed in the chronological order in which the data were taken for this experiment. The maximum number of overlaps ever observed was four. The nonstationary maximum-likelihood estimate of the number of channels in the patch also gave a value of four when the probability of opening was high. The number of openings per record could clearly be much greater than 4, the largest being 20, with values of 9–15 not infrequent.

parameters A and B of model M_1 (see Table III) are also given in Table I. Note that B was most often much smaller than the ACS result of $0.85 < B < 1$. In fact, nonrealizable values ($B < 0$ or $B > 1$) were obtained in >50% of the cases; these are indicated as measurements that are not realizable with the model in the table. Similarly poor results were obtained with model M_2 of Table III. On the other hand, model M_3 or other, more complicated schemes could always be used to

realize these measurements. It should be noted, however, that the models that can realize the measurements have an additional free parameter.

Model parameters were also obtained from average measured quantities, i.e., the number of openings divided by the number of traces and the fraction of failure traces. The results are given in Table II and they compare favorably with those in Table I. The values of $P(0)$ and ρ are given with and without correction for missed fast openings ($P_D = 1$ and $P_D < 1$, respectively), and it is seen that significant differences occurred. The column labeled "$\bar{j}$(|opened)" is particularly

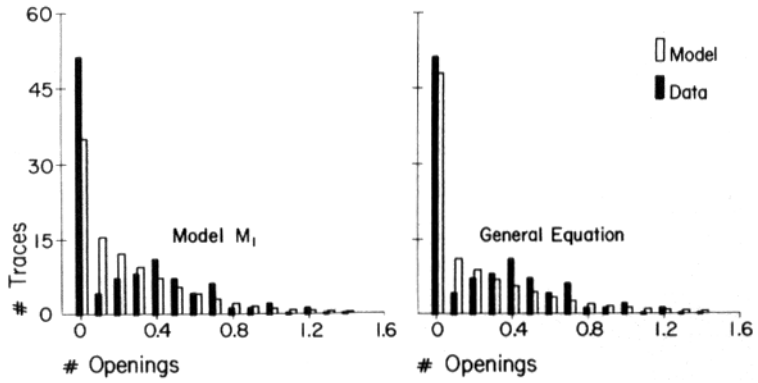

FIGURE 3. Comparison of the fit of model M_1 and the general equation to a distribution of numbers of openings per trace. The filled bars are data and the open bars are model predictions. The fit obtained using the general equation [${}_NP_A(j)$ as given in Eq. 2] was significantly better than that of model M_1, where the parameters were constrained to be realizable (≥ 0 and ≤ 1). Significance was determined by the maximum-likelihood ratio test where -2 times the natural logarithm of the ratio of the maximum likelihoods is approximately distributed as χ^2 (Meyer, 1975; Horn and Lange, 1983). In this case, there is 1 degree of freedom since the number of free parameters was 2 in both cases (see Meyer, 1975) and $\chi^2 = 8.5$. This leads to a rejection ($P \cong 0.001$) of the hypothesis that the fits were the same. The experiment was ID 464 of patch 3 in Table I. The parameters for model M_1 when A and B were constrained were: $A = 0.45$, $B = 0$.

interesting because it shows the average number of openings, given that there was an opening. Note that this number was >1 in all but one case, and it was most often ~2. This result contrasts with that in neuroblastoma cells, where channels almost always opened only once per sample (Aldrich et al., 1983). Once again, the M_1 model could realize the measurements in only 50% of the cases and model M_2 was also unsatisfactory, whereas model M_3, or more complicated models having more than one inactivated state, could realize all the measurements.

The parameters of model M_1, the ACS model, depend on the value of N. Since the range of potentials was limited and peak P_o was small, it was possible that N was underestimated. To study this further, we examined the effect of larger values of N on the parameter values obtained from the measured average

TABLE I

Data						Model parameters					
						General		M_1 model			M_3 model
ID number	Holding potential	Test potential	Number of channels	P_R ($t = 0$)	MOT	$P(0)$	ρ	A	B	Realizable	Realizable
					ms						
(Patch 1)											
501	V_R −50	V_R −20	4	0.45	0.4	0.78	0.74	0.50	−0.48	No	Yes
500		V_R −10			0.7	0.68	0.72	0.30	−0.03	No	Yes
502		V_R +0			1.0	0.75	0.55	0.45	−0.02	No	Yes
503		V_R +10			1.0	0.78	0.38	0.50	0.25	Yes	Yes
602	V_R −70	V_R −30		0.94	0.3	0.87	0.34	0.87	−1.57	No	Yes
601		V_R −20			0.5	0.50	0.54	0.48	−0.03	No	Yes
604		V_R −10			0.65	0.44	0.59	0.40	0.01	Yes	Yes
702	V_R −60	V_R −10		0.73	0.77	0.45	0.52	0.25	0.30	Yes	Yes
700		V_R +0			1.0	0.49	0.39	0.30	0.47	Yes	Yes
701		V_R +10			1.1	0.58	0.24	0.41	0.59	Yes	Yes
(Patch 2)											
470	V_R −50	V_R −10	3	0.45	0.9	0.76	0.63	0.46	−0.17	No	Yes
471	V_R −60			0.73	0.92	0.53	0.40	0.35	0.38	Yes	Yes
472	V_R −70			0.94	1.3	0.58	0.46	0.54	−0.04	No	Yes
(Patch 3)											
462	V_R −50	V_R −10	3	0.45	0.4	0.48	0.45	−0.17	0.61	No	Yes
464		V_R +0			1.0	0.78	0.74	0.50	−0.51	No	Yes
465		V_R +10			1.1	0.75	0.40	0.45	0.27	Yes	Yes
466		V_R +20			1.1	0.73	0.05	0.40	0.92	Yes	Yes
(Patch 4)											
454	V_R −70	V_R −20	3	0.94	1.5	0.84	0.38	0.83	−1.30	No	Yes
453		V_R −10			1.4	0.71	0.11	0.70	0.61	Yes	Yes
452		V_R +0			1.6	0.64	0.40	0.62	−0.07	No	Yes

The table lists parameters from four patches obtained by fitting $P_A(j)$ to distributions such as those in Fig. 2. Values for the initial probability of being in the closed state, P_R ($t = 0$), were estimated as described in the text (see Fig. 5). The measurements were "realizable" with the model if the probabilities (A and B in the case of ACS) are between 0 and 1. Note that in most cases the B's were either small (<0.4) or were nonrealizable with the model. On the other hand, the measurements were realizable in all cases with model M_3.

TABLE II

Measurements								Calculated values ($P_D = 1$)			Calculated values ($P_D < 1$)				Model M_1			Model M_3
ID number	Holding potential	Test potential	Number of channels	P_R ($t = 0$)	MOT	Number of openings: Number of traces	Number of openings: Number of traces	$P(0)$	ρ	$\bar{j}$	$P(0)$	ρ	$\bar{j}$	$\bar{j}(\|\text{open})$	A	B	Realizable	Realizable
					ms													
(Patch 1)																		
501	V_R −50	V_R −20	4	0.45	0.4	2.42	0.414	0.80	0.67	0.61	0.78	0.75	0.88	4.0	0.51	−0.55	No	Yes
500		V_R −10			0.7	3.78	0.232	0.69	0.68	0.94	0.67	0.72	1.2	3.6	0.28	−0.004	No	Yes
502		V_R +0			1.0	1.98	0.320	0.75	0.50	0.49	0.73	0.54	0.57	2.2	0.41	0.09	Yes	Yes
503		V_R +10			1.0	0.697	0.354	0.77	−0.31	0.17	0.72	−0.38	0.20	0.72	0.38	1.62	No	Yes
602	V_R −70	V_R −30		0.94	0.3	0.432	0.705	0.92	0.22	0.11	0.88	0.32	0.18	1.5	0.87	−1.53	No	Yes
601		V_R −20			0.5	3.17	0.140	0.61	0.51	0.79	0.55	0.58	1.1	2.4	0.53	−0.23	No	Yes
604		V_R −10			0.65	4.33	0.092	0.55	0.58	1.1	0.51	0.64	1.4	2.8	0.48	−0.22	No	Yes
702	V_R −60	V_R −10		0.73	0.77	3.73	0.083	0.54	0.50	0.93	0.49	0.55	1.1	2.2	0.30	0.21	Yes	Yes
700		V_R +0			1.0	2.90	0.094	0.55	0.38	0.72	0.51	0.42	0.84	1.7	0.33	0.37	Yes	Yes
701		V_R +10			1.1	1.97	0.156	0.63	0.24	0.49	0.59	0.27	0.56	1.4	0.44	0.52	Yes	Yes
(Patch 2)																		
470	V_R −50	V_R −10	3	0.45	0.90	1.65	0.473	0.78	0.60	0.55	0.76	0.68	0.65	2.8	0.48	−0.23	No	Yes
471	V_R −60			0.73	0.92	1.99	0.172	0.56	0.33	0.66	0.51	0.37	0.78	1.6	0.32	0.46	Yes	Yes
472	V_R −70			0.94	1.3	2.14	0.2	0.58	0.42	0.71	0.56	0.45	0.58	0.80	0.53	0.05	Yes	Yes
(Patch 3)																		
462	V_R −50	V_R −10	3	0.45	0.4	1.49	0.160	0.54	0.08	0.50	0.36	0.12	0.72	1.1	−0.41	0.92	No	Yes
464		V_R +0			1.0	2.65	0.515	0.80	0.77	0.88	0.79	0.80	1.0	5.0	0.55	−0.77	No	Yes
465		V_R +10			1.1	0.907	0.474	0.78	0.27	0.30	0.76	0.30	0.35	1.4	0.46	0.44	Yes	Yes
466		V_R +20			1.1	0.747	0.465	0.77	0.09	0.25	0.74	0.11	0.29	1.1	0.44	0.81	Yes	Yes
(Patch 4)																		
454	V_R −70	V_R −20	3	0.94	1.5	0.664	0.636	0.86	0.37	0.22	0.85	0.39	0.24	1.6	0.84	−1.45	No	Yes
453		V_R −10			1.4	1.20	0.325	0.69	0.22	0.40	0.66	0.24	0.45	1.3	0.64	0.33	Yes	Yes
452		V_R +0			1.6	1.62	0.292	0.66	0.37	0.54	0.64	0.40	0.59	1.7	0.62	−0.05	No	Yes

The table shows the measured average quantities and the model parameters obtained from them. Calculated values are given assuming that all the channels were detected ($P_D = 1$), as well as the realistic case where fast openings are missed ($P_D < 1$) as calculated by the theory in the text. Model parameters are given for the ACS model. These parameters are probabilities and are indicated as being realizable only if they are ≥ 0 and ≤ 1. Note that in 50% of the cases, the ACS model gave nonrealizable values. On the other hand, model M_3 gave realizable values in all cases. The minimum resolvable open time (t_0) in the calculations was 0.15 ms, which corresponds to a 50% threshold and a corner frequency of 1.2 kHz. The value of P_R ($t = 0$) was taken from the $h_\infty(v)$ curves in Fig. 5. Each set of measurements consisted of ~100 traces.

quantities. In Fig. 4, the fraction of failures and the average number of openings for an ensemble of samples were obtained directly from the data, N was varied between 1 and 10, and A and B were calculated. If the results were realizable with model M_1 ($0 < A < 1$ and $0 < B < 1$), then the results were labeled as being consistent with the model. Note that as N increased, the points tended to become inconsistent with the model. Thus, an underestimate of N would not change our conclusion that model M_1 does not apply.

There were other uncertainties. First, our method did not account for missed fast closures, although it did account for missed fast openings. Accounting for the former would tend to increase the number of reopenings, an effect that

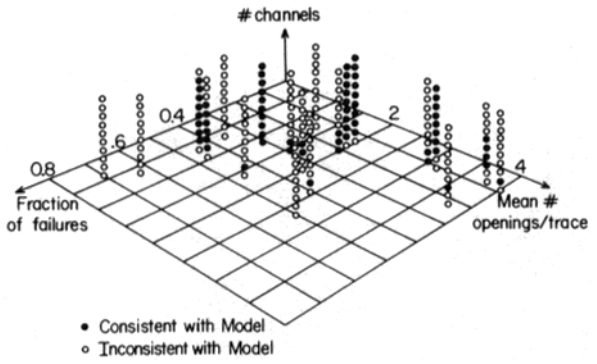

FIGURE 4. Evaluating model M_1, the ACS scheme, as a function of the number of channels in the patch. Using average values obtained from the data, we calculated A and B according to the equations given in the text. The number of openings per trace and the fraction of failure traces were evaluated unambiguously from the data, while the value of N, which is never known with certainty, was varied from 1 to 10, giving the columns in the figure. Each point in a column represents a calculation of A and B. "Consistent" points gave $0 \leq B \leq 1$ and $0 \leq A \leq 1$. "Inconsistent" points gave either larger or smaller values. Several of the "consistent" points may be ruled out since the number of channels was more than three or four in these experiments (Table I). In general, increasing the value of N produced larger inconsistencies with the model M_1. Our conclusions are therefore not changed by an underestimation of N.

would strengthen our conclusion. Another uncertainty was that the resting potential was not measured directly in the cell-attached patches. We assumed it to be near the mean of −60 mV, which is the value we customarily measured in these cells. More support is provided by the fact that the h_∞-potential curves were similar among cell-attached patches in our usual Na solution, among cell-attached patches in isotonic K solution, where the resting potential may be reasonably assumed to be zero (Fig. 5), and among excised patches, where the potential is established with certainty. The asymptote of the h_∞ curve at negative potentials was not measured experimentally. However, if the h_∞ curve maintains the same shape as that measured from the whole cell current, then the asymptote was obtained (Fig. 5). Nevertheless, it is possible that our P_R ($t = 0$) values were overestimated. This, in turn, would lead to an overestimation of A and an

underestimation of B. We evaluated this using the equations associated with model M_1 in Table III and found that after reducing P_R by 15%, there remained several negative B values and the largest B values increased by only ~12%. Such values still do not validate the model.

Slow Inactivation, Waiting Times, and Open Times

Na currents in adult rat myocytes have fast and slow rates of inactivation (Brown et al., 1981*b*; Zilberter et al., 1982). This is also the case in neocytes, as Fig. 6 illustrates. The inward Na current persists for >30 ms at −40 mV, a potential at which the activation and inactivation curves no longer overlap (Fig. 13). It was

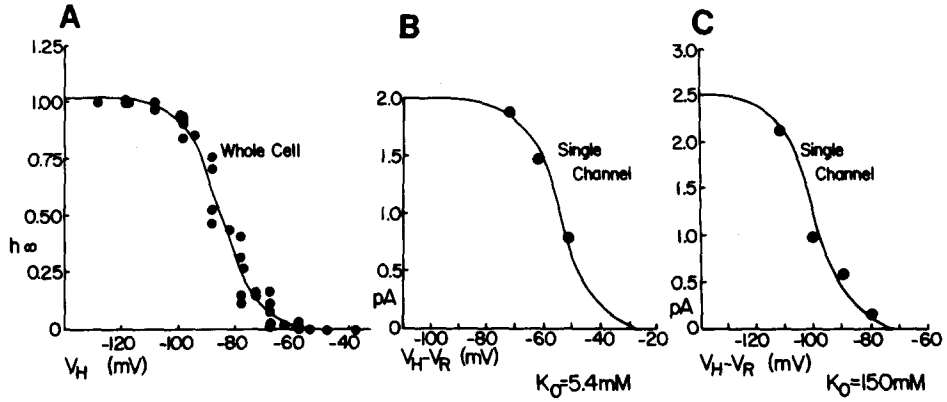

FIGURE 5. Comparison of $h_\infty(v)$ curves from neocyte whole cell and single channel measurements. (*A*) Whole cell $h_\infty(v)$ curve obtained from a double-pulse protocol with a prepulse of 600 ms in duration; the test pulse was to −10 mV. Data points represent five sets of measurements on the same cell taken over 15 min. The smooth curve was described by $h_\infty = [1 + e^{(V-V')/k}]^{-1}$, where the parameters are $V' = -84.7$ mV and $k = 6.49$ mV. (*B*) Single channel $h_\infty(v)$ curve for a cell-attached patch obtained from pulsing to V_R −10 for 30 ms from holding potentials of V_R −50, V_R −60, and V_R −70 mV. The smooth curve used the same expression and parameters used in *A*, except that V' was V_R −51 mV. Assuming a V_R of −60 mV, the usual resting potential of these cells in the normal extracellular solution is equivalent to a shift of ~25 mV. (*C*) Single channel $h_\infty(v)$ curve for a cell-attached patch obtained by pulsing to V_R for 30 ms after holding at V_R −110 when the cell was depolarized to ~0 mV by a bathing solution containing 150 mM KCl.

evident for as long as 15 and 10 ms at −30 and −20 mV, respectively, potentials that are well outside the limits of the overlap. In the overlap zone, the inward Na currents could persist for 100–600 ms as Figs. 6, *B* and *C*, and 7 show. Fig. 7 also shows that these currents are blocked by TTX, which confirms our previous observations in adult myocytes (Brown et al., 1981*b*). The persistence of the Na current occurs at the single channel level as well, and we show later (Fig. 14) that a function that is the sum of two exponentials fits the averaged single channel and whole cell currents with the same two time constants.

The results from neuroblastoma and GH4 cells (Aldrich et al., 1983; Aldrich and Stevens, 1984) showed that the average single channel current could be

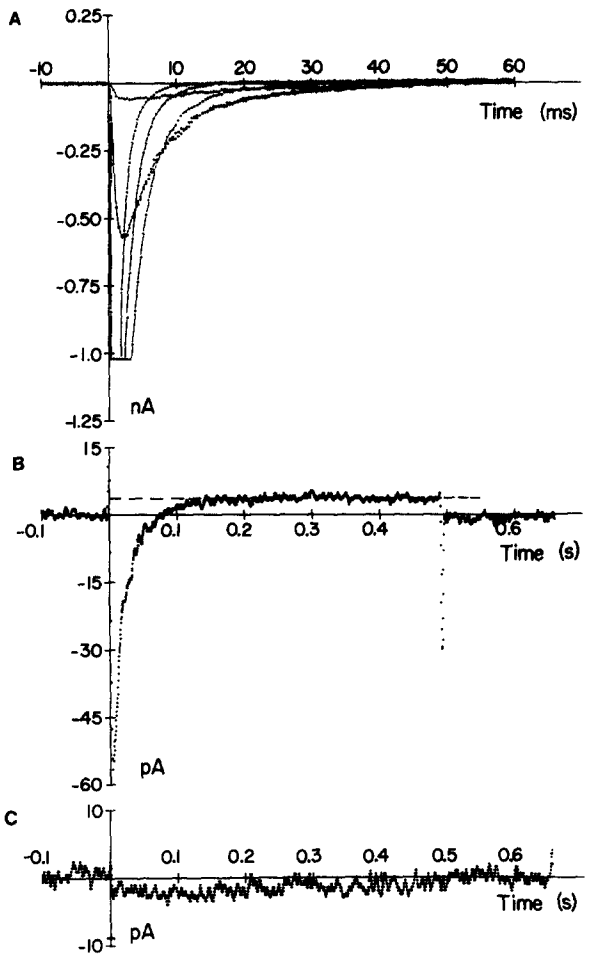

FIGURE 6. Slow inactivation of neocyte whole cell Na currents. The currents produced by 500-ms pulses to −60, −50 (two traces), −40, −30, and −20 mV are shown at several time and amplitude gains. In *A*, the first 60 ms of the current traces is shown. The recording equipment clipped the peak amplitudes of the currents produced by the steps to −40, −30, and −20 mV. Data points have been connected by lines in the initial portions of the records for clarity. The smallest current in *A*, the current produced by the step to −60 mV, is shown in *B* at reduced time gain and increased amplitude gain. A significant current relaxation can be seen at 100 ms. The leakage current produced by the depolarizing step is given by the current level at the end of the pulse and is indicated by the dashed line. Hence, the relaxation is due to an inward Na current. The currents in *A* and *B* have not been corrected for leakage or capacitive currents. In *C*, the very small current caused by a pulse to −71 mV is shown after correction for linear leakage and capacitive current by a hyperpolarizing pulse of equal amplitude to the depolarizing pulse. The current can be seen to inactivate very slowly over the entire pulse. Current traces in *B* and *C* were filtered with a four-pole zero-phase digital filter at a cut-off frequency of 100 Hz, and in *A* with an analog single-pole filter having a corner frequency at 200 Hz. Currents were obtained in a bath solution with 40 mM Na at a holding potential of −100 mV and a temperature of 23°C. These currents were blocked by TTX (5×10^{-5} M).

obtained from the convolution of the open time distribution function and the waiting time probability density function (PDF). We were particularly interested in applying this idea to the slowly inactivating Na currents shown in Fig. 6. For these currents, first openings would have to occur after as long as 600 ms and the cumulative waiting time distribution should be rising steadily during the step depolarization. In fact, this was never observed; rather, the maximum value of this distribution was reached within 10–15 ms. A large time constant for the open time PDF could reconcile the difference. However, in all but two cases to be discussed later, the open time distributions were described by single-exponen-

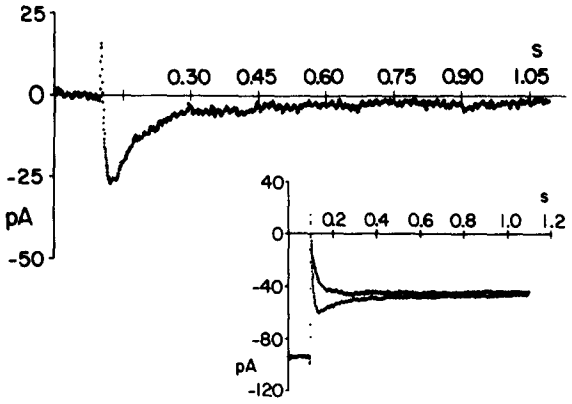

FIGURE 7. TTX-sensitive Na current. Averaged currents for a 1-s pulse from a holding potential of −95 mV to a step potential of −60 mV were obtained first in the absence of TTX and then in the presence of 50 μM TTX. In the inset, the upper trace is the average of currents in the presence of TTX and the lower trace is the average of currents in the absence of TTX. The averaged current in the presence of TTX was subtracted from the averaged current in the absence of TTX to produce the current shown in the main figure. A slowly inactivating process can be observed for 300–600 ms.

tial functions (Fig. 8) with mean values of ~1.0 ms. We also compared the open times between the first and the last openings in each sample and there were no differences. This was true when the respective amplitudes were compared as well. Hence, there was no evidence of the development of time-dependent phenomena in unitary conduction or dwell time in the open state during the processes of activation and inactivation. The absence of long delays in waiting times also excludes the possibility of a set of "sleepy" Na channels such as the ones described by Matteson and Armstrong (1982).

The result obtained from convolving the waiting and open time distributions is compared with $\langle I \rangle_{Na}$, the averaged single channel current in Fig. 8. The waiting time distribution was described by a three-state model (Fig. 8*C*) and corrected for the presence of four channels in the patch. The convolution was only slightly different from the waiting time PDF since the open times were relatively short in comparison (Fig. 8*B*). The convolution was zero at 18 ms, whereas the averaged single channel current persisted for 48 ms of the 60-ms-duration pulse. As expected from the reopenings discussed earlier, the waiting time PDF does not predict the slow inactivation of I_{Na}.

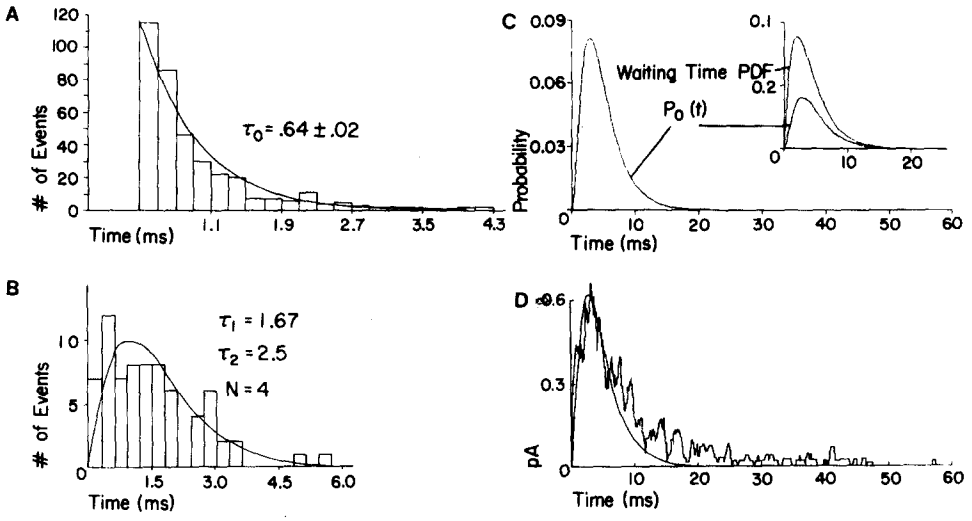

FIGURE 8. Comparison of the averaged single Na channel current with the convolution of the open duration and latency distribution. The waiting time in most cases is not dispersed enough to account for the time course of the current assuming a channel that opens only once. (*A*) Open time distribution fitted with a single exponential PDF having a mean open time of 0.64 ± 0.02 ms. (*B*) The waiting time (WT) histogram was fitted to the time derivative of the waiting time cumulative probability fraction corrected for N channels (Patlak and Horn, 1983).

$$\mathrm{WT}_{\mathrm{cpf}} = 1 - \left(- \frac{\rho_2}{\rho_1 - \rho_2} e^{-\rho_1 t} + \frac{\rho_1}{\rho_1 - \rho_2} e^{-\rho_2 t} \right)^N .$$

This is the form of the expression expected for a three-state model of activation and the ρ's are inverse time constants. The number of channels was four, the time constant parameters are shown, the total number of events measured was 76, and the number of failures was 23. (*C*) The probability of opening, $P_o(t)$, was calculated from the convolution of the waiting time PDF for one channel with the probability that a channel is open at time t given that it was open at time 0 (Aldrich et al., 1983). The $P_o(t)$ curve was scaled appropriately for the failure rate. Also shown in the inset is the waiting time PDF and one sees that $P_o(t)$ is only a slightly "smeared" version of the former, as would be expected from a mean open time of 0.64 ms. The convolution was done numerically using the result that convolution in the time domain is equivalent to multiplication in the Laplace domain. We obtained Laplace transforms of the expressions for waiting time PDF and e^{-t/τ_o} and multiplied them together. This result was inverse Laplace transformed using a general numerical inversion algorithm to obtain the $P_o(t)$ curve. Mathematical functions describing the waiting and open times were used rather than raw data because the waiting time raw data distribution was extremely "noisy" after correction for $N = 4$. This will introduce error, but probably not enough to change the conclusion. An interesting property of the waiting time PDF can be observed by comparing the curve for one channel shown in the inset with the fitted curve for four channels shown in *B*. Noting the difference in time bases, the curve for four channels is very much "faster" than that for one channel, as expected. (*D*) The time course of the average currents from this patch is compared with the smooth curve $P_o(t)$ for one channel as calculated in *C*. Note that the current remains nonzero significantly longer than the $P_o(t)$ curve, which is consistent with extensive reopening shown in Fig. 2.

Shifts in the Inactivation-Potential Relation

At $V_H = V_R$ −50 mV and V_{step} = 50 mV, the sweeps with zero openings (nulls or failures) were more frequent than when the membrane was hyperpolarized further and stepped to the same test potential. Between V_R −60 mV and V_R −70 mV, the number of failures changed only slightly, which suggests that at these potentials, h_∞ was approaching 1. A more accurate test is a comparison of the average current from summed records at the same test potential and different conditioning potentials. From this comparison, the h_∞-potential relation shown in Fig. 5 was obtained. The usual resting potential of these dispersed neonatal myocytes in the present solutions was −50 to −60 mV, so that h_∞ was 0.5 at about −100 mV. Values for the $V_{0.5}$ of h_∞ of −100 mV were also obtained when the extracellular solution contained isotonic K, in which case the resting potential was probably zero or close to that value. However, in intact neocytes, the potential at which h_∞ became 0.5 was −85 mV (Fig. 5). This value showed a small, gradual change throughout the period of whole cell recording (Marty and Neher, 1983; Fernandez et al., 1984), whereas when a patch of membrane was clamped, the h_∞-potential curves moved toward more negative values within a few minutes of establishing the patch and then remained stable. This time sequence was true for excised patches as well. Threshold for activation in intact neocytes was about −70 mV and was shifted in the hyperpolarizing direction for both cell-attached patches and excised patches by an amount that was similar to the shift in the $V_{0.5}$ of the h_∞-potential relation. Our results confirm that gating was shifted in excised patches as reported by Cachelin et al. (1983), but, in addition, they showed that such shifts could occur in cell-attached patches.

Single Na Channel I-V Relation

The single channel *I-V* relation (Fig. 9) had a maximum slope conductance of ~20 pS, in agreement with other results (Sigworth and Neher, 1980; Cachelin et al., 1983; Grant et al., 1983). At hyperpolarizing potentials, the *I-V* curve became flat. A similar observation was reported by Grant et al. (1983). The instantaneous *I-V* curve measured from tail current amplitudes showed a similar flattening. We cannot exclude the possibility that the flattening resulted from the limited recording bandwidths of the single channel (1–1.5 kHz) and whole cell (10.0 kHz) methods rather than from a property of the channel itself. This is suggested by the fact that the mean open time (MOT) became very small and tail currents became very fast at hyperpolarized potentials. However, Yamamoto et al. (1983) have shown that Ca can modify single channel Na *I-V*'s in a similar manner.

We noted, as did Cachelin et al. (1983), that occasionally there was evidence for two populations of unitary amplitudes (Fig. 10). The open time distribution in these cases was fitted best by the sum of two exponentials and the smaller amplitudes had the briefer duration. The larger-amplitude events had the same amplitude and duration distributions as the events we usually recorded and appeared to be by far the more frequently occurring channel. The smaller, briefer unitary events were seen too infrequently to be studied extensively. Nagy et al. (1983) made similar observations on Na channels of mouse neuroblastoma cells and concluded that there were two sets of Na channels. A contribution from

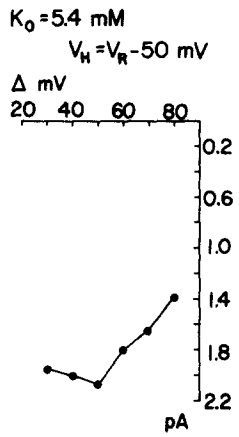

FIGURE 9. Single channel *I–V* relation for a cell bathed in the normal extracellular solution. The *I–V* curve became flat at the more negative potentials. The conductance calculated for the portion between −50 and −80 mV was 24 pS.

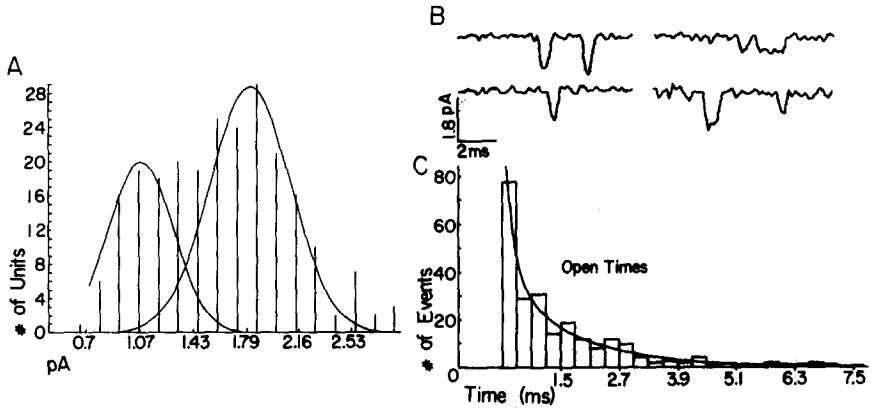

FIGURE 10. Two populations of Na channels. (*A*) An example of bimodal amplitude distribution obtained from a holding potential of V_R −50 with a step depolarization of 50 mV and 30 ms duration. The data were fitted with two Gaussian functions, having means of 1.02 and 1.7 pA and standard deviations of 0.2 and 0.25 pA. (*B*) Single channel records selected from samples of the same ensemble that illustrate the two amplitudes. (*C*) Open time distribution obtained on data from this patch. The smooth curve is from a two-exponential PDF that fitted the data significantly better than a one-exponential PDF as determined by the maximum-likelihood ratio test. There were 2 degrees of freedom and χ^2 was 15.2, which led to a rejection ($P \cong 0.0005$) of the hypothesis that fits were the same (see Fig. 3). The number of open intervals was 238. The biexponential equation was

$$\text{OP PDF} = \frac{A_1}{\tau_1} e^{-t/\tau_1} + \frac{(1 - A_1)}{\tau_2} e^{-t/\tau_2},$$

where $A_1 = 0.54$, $\tau_1 = 0.17$ ms, and $\tau_2 = 1.5$ ms.

T-system Na channels can be excluded in our experiments since these neocytes lacked T-systems (Lacerda et al., manuscript in preparation).

Neocyte Whole Cell Na Currents and the Question of a Separate Set of Threshold Na Channels in the Heart

Our experiments were performed at potentials between threshold and the plateau of the cardiac action potential in rat (Josephson et al., 1984). Therefore, we were interested in the possibility that threshold currents, such as those described by Gilly and Armstrong (1984), having slow tail components at return potentials equal to the resting potential might be present. A prediction from these experi-

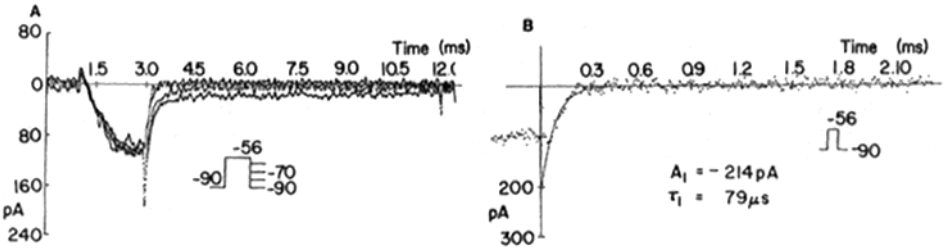

FIGURE 11. Tail currents at threshold potentials. In *A*, currents arising from a series of pulses to a constant potential in the threshold range of Na channel gating and varied return potentials are shown superimposed. The pulse protocol is shown in the inset in *A*. No slow current relaxation can be seen in the tail currents when the return potential was −90 mV, the holding potential, or −80 mV. A slow relaxation is evident at a return potential of −70 mV and it is slower and larger at the −60-mV return potential. The zero-current level can be seen as the current after the artifact at 12 ms when the return potential was brought back to a holding potential of −90 mV. The current components revealed at return potentials of −70 and −60 mV, respectively, are due to activation and slow inactivation of Na channels at these return potentials. A single-exponential fit to the tail current at a return potential of −90 mV is shown in *B*. The fit to the tail current had an initial amplitude of −214 pA and a time constant of 79 μs. For return potentials to −80, −70, and −60 mV, the deactivation tail τ's were 98, 120, and 88 μs, respectively. Data were filtered at 15 kHz by a two-pole, zero-phase digital filter; the temperature was 24°C.

ments is the occurrence of a separate population of threshold Na channels with prolonged open times, which could cause the slow tail currents. However, the open time distributions for records containing only a single amplitude distribution were monoexponential, and the infrequent smaller-amplitude events cannot be implicated since their durations are briefer. Whole cell currents were recorded using holding, test, and return potentials analogous to those that produced a well-defined, slow inward tail current in squid axon. No such tail current was present in neocytes (Fig. 11). The tail currents relaxed with a single time constant that was <100 μs. However, when the return potential was in the range of the threshold potential, between −70 and −60 mV, the tail currents showed a slow component (Fig. 11*A*) caused by activation of channels that were not inactivated during the preceding test pulse to potentials just above the threshold range.

We examined I_{Na}'s over a wide range of potentials as part of a more complete study in which I_{Na}'s of neonatal and adult rat ventricular myocytes will be compared (Lacerda et al., manuscript in preparation). Fig. 12 shows the peak *I–V* curve for the neocyte Na current shown in the inset. This is simply a scaled version of the *I–V* curve of an adult rat cardiac myocyte (Brown et al., 1982). Both are blocked by TTX at concentrations of 5×10^{-5} M. The $h_\infty(v)$ and $m_\infty(v)$ relations are shown in Fig. 13. They are also similar to the relations for adult cardiac myocytes that have been reported (Brown et al., 1982).

The waveforms of the averaged single channel and whole cell currents resem-

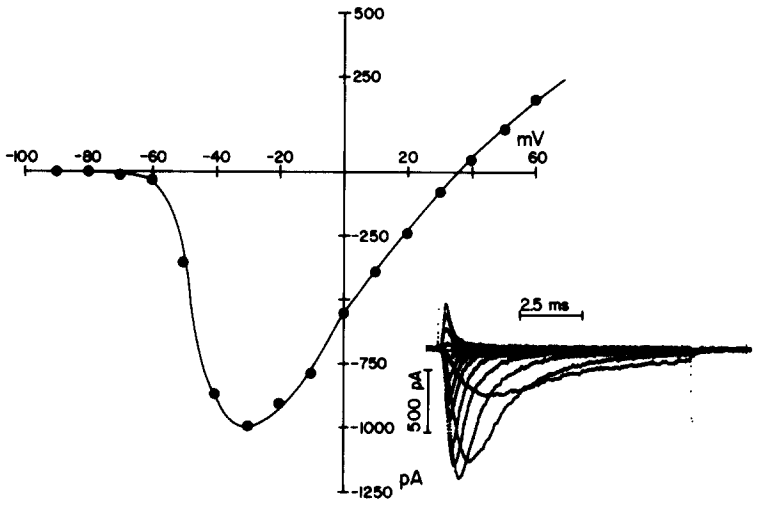

FIGURE 12. *I–V* relation for Na currents. Whole cell *I–V* relation and currents (inset) for TTX-sensitive Na currents are shown for a neocyte bathed in 40 mM external Na. The intracellular pipette contained (in mM): 120 CsCl, 10 NaCl, 1 CaCl, 11 EGTA, 2 $MgCl_2$, 10 glucose, 10 HEPES (pH 7.2). The calculated Na reversal potential of 35 mV agrees with the measured reversal potential. This also agrees with the extrapolated reversal potential for the single channel *I–V* relation shown in Fig. 8. Currents caused by pulses from −50 to +60 mV are shown in the inset and have been corrected for leakage and capacity transients. Data were filtered at 10 kHz with a two-pole, zero-phase digital filter; the temperature was 22°C.

bled each other at potentials that were similar. It should be noted that there is some uncertainty about holding and test potentials for cell-attached patches. Fits were made with a model having two inactivation components (Fig. 14) and showed that similar parameters fitted both curves. In an earlier report (Brown et al., 1981*b*), we demonstrated that Na currents in adult rat ventricular myocytes inactivated at two different rates. Patlak (1984) has reported two inactivation rates for averaged single Na channel currents in cardiac myocytes that could be modified by changes in holding potential. The present observations on single channels are of interest because the Na channels from which the average current was computed had a unimodal amplitude distribution and a single-exponential

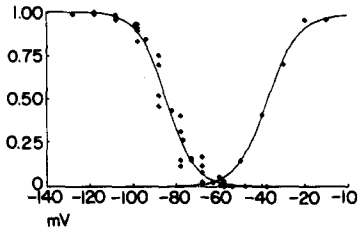

FIGURE 13. Activation and steady state inactivation of Na channels. The $h_\infty(v)$ relation (descending curve) for whole cell currents shown in Fig. 5 is shown here with activation data (ascending curve) obtained from a different cell. Activation was measured as the fitted initial amplitude of the tail current at the end of brief pulses to activating potentials. The $h_\infty(v)$ curve was fitted using the function described in the legend to Fig. 5. The activation curve was fitted with the same function, except that the form constant was negative.

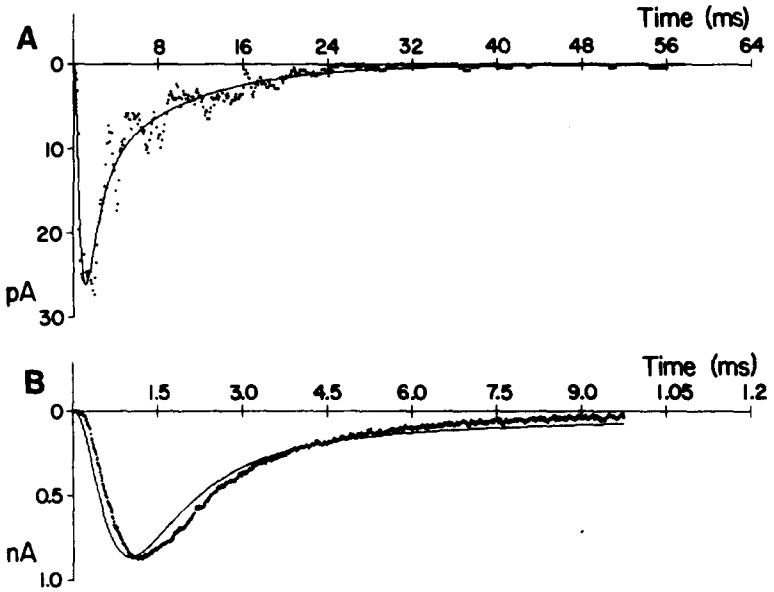

FIGURE 14. Comparison of summed single channel and whole cell currents. Summed single channel currents shown in *A* are fitted using a modified H-H expression with two inactivation components, i.e., $I = A(1 - e^{-t/\tau}m)^3[(1 - s)e^{-t/\tau}h_1 + se^{-t/\tau}h_2]$. The whole cell current in *B* is fitted by the same model. Note differences in time bases. The fitting program was allowed to vary only the peak value of the current and the fraction of current exhibiting a slow relaxation in *B*. τ_m, τ_{h_1}, and τ_{h_2} were fixed at the values obtained from the fit to the summed single channel currents in *A* and were 0.45, 1.25, and 8.8 ms, respectively, and s was 0.23. The whole cell current was obtained in 40 mM Na at a pulse potential of −40 mV. The single channel currents were recorded from a cell-attached patch; the holding potential was V_R −50 mV and the step amplitude was 70 mV.

open time distribution, which were consistent with the usual results obtained in our experiments; i.e., the second set of Na channels was not present in this patch. The result is therefore direct evidence that the predominant single Na channel has two rates of inactivation.

DISCUSSION

The present results show that Na channels reopen sufficiently to produce slow inactivation. The latter can clearly contribute to the plateau of the cardiac action potential, although the quantitative contribution is uncertain. Changes in action potential duration associated with changes in heart rate may involve this process, as may the use and voltage dependence of local anesthetics. The effect is not due to a window current and implies more than one inactivated state. In an earlier study in adult rat ventricular myocytes (Brown et al., 1981*b*), we showed that an $m^3(h_1 + h_2)$ model having two inactivated states in parallel could fit the data and we have confirmed this here. However, we have not excluded a model such as the one proposed for axonal Na currents by Chiu (1977), in which the inactivation kinetics are second order; i.e., the two inactivated states are in series. In fact, our earlier results (Brown et al., 1981*b*; Figs. 9 and 10) showed that recovery from inactivation occurred after a small delay, a result that favors the in-series model. Another possibility is the suggestion by Patlak and Ortiz (1985) that Na channels may operate in different or heterogeneous modes. We cannot address this possibility at present since we have not observed samples containing prolonged bursts and a high opening probability such as those described by Patlak and Ortiz at room temperature; however, similar but infrequent observations were made at 10°C. In addition, we have not observed a cross-over of the inactivating currents when the holding potential was changed from −90 to −130 mV, although in our experiments the $h_\infty(v)$ relation reached 1.0 at −120 mV.

The Na channels we recorded most frequently had conductances and durations similar to those described for neocyte Na channels by Cachelin et al. (1983). They found, as we did, evidence of a second set of Na channels. Given the brief average open duration of these channels, it is possible that their lower amplitude reflects the bandwidth limitations of the recording system. However, we did observe long openings of equally small amplitudes and, although they were observed infrequently, they were present in patches that also contained the predominant channel type. We cannot evaluate the role of these channels in slow inactivation, but the process was evident in their absence and is a property of the predominant Na channel type. We could also find no evidence of a separate set of threshold Na channels that might give rise to window or slowly inactivating Na currents.

A major difference between our results on single cardiac Na channels and those described recently for single Na channels in neuroblastoma and GH4 cells (Aldrich et al., 1983; Aldrich and Stevens, 1984) was the larger number of openings observed in our samples. As a result, in our case, the B parameter of the ACS model tended to be <0.4, whereas in the case of the ACS model, it was >0.85. Our results indicated more reopenings than those obtained by the ACS model; we calculated that if the channels opened, they tended to open ~1.5–5

times (Table II). Not only did we get different parameter values than the ACS model, we also obtained many measurements that were not reconcilable with the ACS scheme (Tables I and II). That is, the probability parameters A and B were often <0 or >1 and were therefore not physically realizable with the model. Similar results were sometimes obtained by Vandenberg and Horn (1984) when they evaluated the ACS model on their data in GH3 cells. Model M_2 would also not describe the results. Unlike these models, model M_3 could realize our measurements (but see below). Another prediction of the ACS model was the convolution test on the waiting and open time data. The expected time course did not describe the measured $P_o(t)$, again because of reopening. These differences may not be surprising considering that ventricular Na channels have a slow component of inactivation.

The method used here for evaluating models based on the number of openings per sample would seem to be a useful preliminary analysis technique. Note that this analysis accounted for missed fast openings and that this was an appreciable effect (Table II). The analysis pointed out that model M_3, or other, more complicated models that may have two inactivated states, could realize the measurements, whereas models M_1 and M_2 could not. However, we have not rigorously tested other, more complicated models for the reasons given below. We should also point out that the method used here does not take into account all the information regarding the number of openings recorded. For example, a trace having three overlapping openings is not treated any differently from a trace having three noncoincident openings. Obviously, the latter gives a suggestion of reopening, while the former does not. A significant problem was that we always obtained more than one channel in our patches. Given this complication, it is difficult to proceed much further in testing state models using single channel interval analysis without resorting to much more complicated techniques such as the maximum-likelihood method of Horn and Lange (1983).

Horn and Vandenberg (1984) fit 25 different state models to their Na channel data from GH3 cells and ranked them statistically. In a companion paper (Vandenberg and Horn, 1984), they used one of the simpler models and found that it could describe their single channel inactivation data reasonably well. This model has exactly the same predictions for the number of openings per trace as does our model M_1 and thus would suffer from the same inconsistency with our data. Horn and Vandenberg (1984) tested some other schemes similar to our model M_3 in that the pathway to channel failure did not include a state adjoining the open state. However, there was no model having this property that could be directly compared with their simplified scheme using their statistical ranking. Given our results here, it would be interesting to make such a comparison. This is made more pertinent by the fact that Vandenberg and Horn (1984) occasionally also obtained nonrealizable values when they subjected their data to the ACS analysis.

Our results confirm the observations of Cachelin et al. (1983), Grant et al. (1983), and Fernandez et al. (1984) that the gating of cardiac Na channels is shifted in excised patches. These effects were attributed to the absence or lack of some cytoplasmic factor (Cachelin et al., 1983), but the present observations

of a similar shift in the cell-attached case suggest that this is not the case and that a structural change may be involved.

APPENDIX A

Development of a General Model for the Number of Openings per Trace and Its Relationship to Some State Models of Interest

A General Model

The number of openings per depolarization will be derived for a homogeneous, or linear, Markovian state model with a single open state and an absorbing state, or states. For this problem, after any opening in a trace there are two events of interest: either the channel "reopens," or it "inactivates" and never opens again during the depolarization. For a model as described above, the probabilities of these two events are constant and they are set equal to ρ and $1 - \rho$, respectively. We define $P(j|\text{opened})$ to be the probability that a channel opens j times in a depolarization, given that it has opened. Thus, $P(1|\text{opened})$ is given by the probability that the channel "inactivates," and it equals $1 - \rho$. $P(2|\text{opened})$ is given by the probability of the two independent events, that the channel "reopens" and "inactivates"; thus, $P(2|\text{opened}) = \rho(1 - \rho)$. Similarly, $P(3|\text{opened}) = \rho^2(1 - \rho)$. In general, one obtains

$$P(j|\text{opened}) = (1 - \rho)\rho^{j-1}, \qquad j = 1, 2, \ldots \tag{A1}$$

In addition to the above conditional probability, we are interested in $P(j)$, the probability of j openings per trace. From the requirement that both of these discrete probability distributions must sum to 1, we have $P(0)$ and

$$P(j) = [1 - P(0)]P(j|\text{opened}), \qquad j = 1, 2, \ldots \tag{A2}$$

The averaged quantities given below are obtained from the above and the identity $\sum_{j=1}^{\infty} jh^j = h(1 - h)^{-2}$ for $|h| < 1$.

$$\bar{j}(|\text{opened}) = \sum_{j=1}^{\infty} jP(j|\text{opened}) = \frac{1}{1 - \rho}; \tag{A3}$$

$$\bar{j} = [1 - P(0)]\bar{j}(|\text{opened}) = \frac{[1 - P(0)]}{1 - \rho}. \tag{A4}$$

Some Specific State Models

We will relate some simple state models to the general results shown above. In Table III, state models and what we will call Markov chain diagrams (see later) are given for some simple schemes. This list includes a generalized ACS diagram (model M_1) with multiple closed states proceeding from the left. Note that this scheme includes a model favored by Horn and Vandenberg (model 15 of Table II, Horn and Vandenberg, 1984; Vandenberg and Horn, 1984). The other schemes in the table are included because they give different predictions for the number of openings per trace.

Results will be derived relating model M_3 to the general equation above; other results are obtained analogously. The Markov chain diagram is obtained from the state diagram in the following manner. The probability of making a transition from state O to I is given by $B = k_{OI}(k_{OI} + k_{OC})^{-1}$, where k_{OI} is the rate constant for transitions from O to I, etc. In terms of the number of openings per trace, sojourns among states R through C_{n-1} have no effect on the final result; thus, these states are lumped together, giving R in the Markov

chain diagram. The probability of transitions A and E is given by the ratios of the rate constants as given above for B.

Continuing with the derivation from Eq. A1, a useful quantity is the probability that a channel inactivates after opening only once, and it is $P(1|\text{opened}) = 1 - \rho$. From the Markov chain diagram, this probability is given by the sum of the probabilities for traversing the possible pathways as indicated below.

$$\begin{aligned} P(1|\text{opened}) &= \text{Prob}(O \rightarrow I) + \text{Prob}(O \rightarrow C \rightarrow R \rightarrow I) \\ &\quad + \text{Prob}(O \rightarrow C \rightarrow R \rightarrow C \rightarrow R \rightarrow I) + \ldots \\ &= B + \sum_{m=0}^{\infty} (1 - B)(1 - E)A[(1 - A)(1 - E)]. \end{aligned} \tag{A5}$$

TABLE III

Name	State diagram	Markov chain diagram	Equations
M_1	$R \rightleftharpoons C_1 \cdots \rightleftharpoons C_n \rightleftharpoons O$, $C_n \rightarrow I$	$R \underset{1-B}{\overset{1-A}{\rightleftharpoons}} O$, $R \xrightarrow{A} I$, $O \xrightarrow{B} I$	$\rho = (1 - A)(1 - B)$, $f = A$
M_2	$R \cdots \rightleftharpoons C_{n-1} \rightleftharpoons C_n \rightleftharpoons O$, $C_n \rightarrow I$	$R \underset{B}{\overset{1}{\rightleftharpoons}} C_n \xrightarrow[1]{1-A-B} O$, $C_n \xrightarrow{A} I$	$\rho = 1 - \frac{A}{1-B}$, $f = \frac{A}{1-B}$
M_3	$R \cdots \rightleftharpoons C_{n-1} \rightleftharpoons C_n \rightleftharpoons O$, $C_{n-1} \rightarrow I$, $C_n \rightarrow I$	$R \underset{1-E}{\overset{1-A}{\rightleftharpoons}} C_n \underset{1-B}{\overset{E}{\rightleftharpoons}} O$, $R \xrightarrow{A} I$, $O \xrightarrow{B} I$	$\rho = \frac{E(1-B)}{E + A(1-E)}$, $f = \frac{A}{E + A(1-E)}$

In each diagram, R is the rest state, the C's are additional short-lived closed states, O is the open state, and I is an absorbing inactivated state. The parameters A, B, and E in the Markov chain diagrams are probabilities for the transitions shown. As described in the text, equations on the right are easily obtained from such diagrams.

Using the identity $\sum_{m=0}^{\infty} h^m = (1 - h)^{-1}$ for $|h| < 1$ and rearranging, one obtains

$$\rho = \frac{E(1 - B)}{E + A - AE}. \tag{A6}$$

The channel will fail to open if it is already inactivated (because of the holding potential) or if it goes inactivated without entering the open state. These two cases are included in the expression below where P_R ($t = 0$) is the probability of being in the rest state initially (h_∞ in Hodgkin-Huxley notation) and where f is the probability that a channel fails to open given that it starts in the rest state.

$$P(0) = 1 - P_R\ (t = 0) + fP_R\ (t = 0). \tag{A7}$$

In the case of model M_3, there are several pathways by which such a failure may occur, i.e.,

$$\begin{aligned} f = {} & \text{Prob}(R \rightarrow I) + \text{Prob}(R \rightarrow C \rightarrow R \rightarrow I) \\ & + \text{Prob}(R \rightarrow C \rightarrow R \rightarrow C \rightarrow R \rightarrow I) + \ldots \\ = {} & \sum_{m=0}^{\infty} A[(1 - A)(1 - E)]^m = \frac{A}{E + A(1 - E)}. \end{aligned} \tag{A8}$$

The pertinent equations for M_3 are A6–A8. For the other state diagrams, Eq. A7 and the equations given in Table III are used.

The parameters for the general model, $P(0)$ and ρ (Eq. 1), can be obtained from the data. Using these and the measured value of P_R $(t = 0)$, one can obtain ρ and f, which are in turn related to the model parameters in Table III. For the case of model M_1, there are two unknown parameters (A and B), and they can be uniquely obtained from ρ and f. Model M_2 has the interesting property that $\rho = 1 - f$; thus, it can be directly checked from these two values. Model M_3 has three unknown probabilities; thus, it remains to be seen whether A, B, and E can be obtained with the constraints that $0 < A < 1$, $0 < B < 1$, and $0 < E < 1$. Most other schemes that one might envision would have more than two unknown probability parameters, and they would be handled similarly to M_3.

APPENDIX B

Correction for Missing Fast Openings

We will derive results for the apparent number of openings per trace when fast openings are missed. It is assumed that the underlying true openings are given by Eq. 1. It is also assumed that there is a constant probability of detection, P_D, which is calculated from $\exp(-t_0/\tau_0)$, where t_0 is the system dead time and τ_0 is the mean open time (Colquhoun and Sigworth, 1983). It is assumed that no fast closures are missed that would complicate the analysis (Wilson and Brown, 1985).

An apparent failure trace is obtained from a trace having no true openings, or a trace having one true opening that is missed, or a trace having two true openings that are both missed, etc. Thus, the probability of obtaining zero apparent openings is

$$P_A(0) = P(0) + \sum_{v=1}^{\infty} \text{Prob}(v \text{ missed} | v \text{ true}) P(v), \tag{B1}$$

where Prob(v missed|v true) is the probability of v missed openings given that there were v true openings, and is evaluated using the binomial equation as shown below. Similarly, for j apparent openings, we have

$$P_A(j) = \sum_{v=0}^{\infty} \text{Prob}(v \text{ missed}/j + v \text{ true}) P(j + v) \qquad j = 1, 2, \ldots \tag{B2}$$

where

$$\begin{aligned} & \text{Prob}(v \text{ missed} | j + v \text{ true}) \\ & = \frac{(j + v)!}{v!j!} (1 - P_D)^v P_D^j \\ & = \frac{(v + 1)(v + 2) \ldots (v + j)(1 - P_D)^v P_D^j}{j!} \qquad \begin{matrix} j = 1, 2, \ldots \\ v = 0, 1, \ldots \end{matrix} \end{aligned} \tag{B3}$$

and which is, for the particular case of $j = 0$,

$$\text{Prob}(v \text{ missed} \mid v \text{ true}) = (1 - P_D)^v P_D^j. \tag{B4}$$

Substituting Eqs. 1 and B3 into B2 and rearranging, one obtains

$$P_A(j) = \frac{P_D^j(1 - \rho)[1 - P(0)]\rho^j}{j!\rho} \sum_{v=0}^{\infty} (v + 1)(v + 2) \ldots (v + j)[(1 - P_D)\rho]^v. \tag{B5}$$

Using the identity

$$\sum_{v=0}^{\infty} (v + 1)(v + 2) \ldots (v + j)Z^v = \frac{j!}{(1 - Z)^{j+1}}, \qquad |Z| < 1, \tag{B6}$$

which can be obtained following a suggestion by Knopp (1956), one obtains

$$P_A(j) = \frac{[1 - P(0)](1 - \rho)}{\rho[1 - \rho + \rho P_D]} \left(\frac{\rho P_D}{1 - \rho + \rho P_D}\right)^j \qquad j = 1, 2, \ldots \tag{B7}$$

and using an identity given earlier, the result $P_A(0)$ is obtained.

$$P_A(0) = P(0) + \frac{[1 - P(0)](1 - \rho)(1 - P_D)}{1 - \rho + \rho P_D}. \tag{B8}$$

Finally, the average number of apparent openings can be evaluated using the above relations; the trivial result is

$$\bar{j}_A = \sum_{j=0}^{\infty} jP_A(j) = P_D\bar{j}. \tag{B9}$$

We thank Ms. Lynette Morgan for help in preparing the manuscript and Ms. Cindy Orlea for help with the illustrations.

This work was supported by National Institutes of Health grants HL25145, NS11453, and HL27116.

Original version received 15 October 1984 and accepted version received 8 May 1985.

REFERENCES

Aldrich, R. W., D. P. Corey, and C. F. Stevens. 1983. A reinterpretation of mammalian sodium channel gating based on single channel recording. *Nature (Lond.).* 306:436–441.

Aldrich, R. W., and C. F. Stevens. 1984. Inactivation of open and closed sodium channels determined separately. *Cold Spring Harbor Symp. Quant. Biol.* 48:147–153.

Attwell, D., I. Cohen, D. Eisner, M. Ohba, and C. Ojeda. 1979. The steady state TTX-sensitive ("window") sodium current in cardiac Purkinje fibres. *Pflügers Arch. Eur. J. Physiol.* 379:137–142.

Bard, Y. 1974. Nonlinear Parameter Estimation. Academic Press, Inc., New York. 341 pp.

Bodewei, R., S. Hering, B. Lemke, L. V. Rosenshtraukh, A. I. Undrovinas, and A. Wollenberger. 1982. Characterization of the fast sodium current in isolated rat myocardial cells: simulation of the clamped membrane potential. *J. Physiol. (Lond.).* 325:301–315.

Brown, A. M., K. S. Lee, and T. Powell. 1981*a*. Voltage clamp and internal perfusion of single rat heart muscle cells. *J. Physiol. (Lond.).* 318:455–477.

Brown, A. M., K. S. Lee, and T. Powell. 1981*b*. Sodium current in single rat heart muscle cells. *J. Physiol. (Lond.).* 318:479–500.

Brown, A. M., K. S. Lee, and T. Powell. 1982. Sodium currents in heart muscle. *In* Normal

and Abnormal Conduction in the Heart. A. P. de Carvalho, B. G. Hoffman, and M. Lieberman, editors. Futura Publishing Co., Mt. Kisco, NY. 181–188.

Brown, A. M., H. D. Lux, and D. L. Wilson. 1984. Activation and inactivation of single calcium channels in snail neurons. *J. Gen. Physiol.* 83:751–769.

Cachelin, A. B., J. E. DePeyer, S. Kokubun, and H. Reuter. 1983. Sodium channels in cultured cardiac cells. *J. Physiol. (Lond.).* 340:389–401.

Chiu, S. Y. 1977. Inactivation of sodium channels: second order kinetics in myelinated nerve. *J. Physiol. (Lond.).* 273:573–596.

Colatsky, T. J. 1980. Voltage clamp measurements of sodium channel properties in rabbit cardiac Purkinje fibres. *J. Physiol. (Lond.).* 305:215–234.

Colquhoun, D., and F. J. Sigworth. 1983. Fitting and statistical analysis of single-channel records. *In* Single-Channel Recording. B. Sakmann and E. Neher, editors. Plenum Press, New York. 191–263.

Coraboeuf, E., E. Deroabaix, and A. Coulombe. 1979. Effect of tetrodotoxin on action potentials of the conduction system in dog heart. *Am. J. Physiol.* 236:H561–H567.

Dudel, J., K. Peper, R. Rudel, and W. Trautwein. 1967. The effect of tetrodotoxin on the membrane current in cardiac muscle. *Pflügers Arch. Eur. J. Physiol.* 295:213–226.

Ebihara, L., and E. A. Johnson. 1980. Fast sodium current in cardiac muscle. A quantitative description. *Biophys. J.* 32:779–790.

Fenwick, E. M., A. Marty, and E. Neher. 1982. Sodium and calcium channels in bovine chromaffin cells. *J. Physiol. (Lond.).* 331:599–635.

Fernandez, J. M., A. P. Fox, and S. Krasne. 1984. Membrane patches and whole-cell membranes: a comparison of electrical properties in rat clonal pituitary (GH_3) cells. *J. Physiol. (Lond.).* 356:565–585.

Fukushima, Y. 1981. Identification and kinetic properties of the current through a single Na^+ channel. *Proc. Natl. Acad. Sci. USA.* 78:1274–1277.

Gilly, W. F., and C. M. Armstrong. 1984. Threshold channels—a novel type of sodium channel in squid giant axon. *Nature (Lond.).* 309:448–450.

Gintant, G. A., N. B. Datyner, and I. S. Cohen. 1984. Slow inactivation of a tetrodotoxin-sensitive current in canine cardiac Purkinje fibers. *Biophys. J.* 45:509–512.

Grant, A. O., C. F. Starmer, and H. C. Strauss. 1983. Unitary sodium channels in isolated cardiac myocytes of rabbit. *Circ. Res.* 53:823–829.

Hamill, O. P., A. Marty, E. Neher, B. Sakmann, and F. J. Sigworth. 1981. Improved patch-clamp techniques for high-resolution current recording from cells and cell-free membrane patches. *Pflügers Arch. Eur. J. Physiol.* 391:85–100.

Hodgkin, A. L., and A. F. Huxley. 1952. A quantitative description of membrane current and its application to conduction and excitation in nerve. *J. Physiol. (Lond.).* 117:500–544.

Horn, R., and K. Lange. 1983. Estimating kinetic constants from single channel data. *Biophys. J.* 43:207–223.

Horn, R., and C. A. Vandenberg. 1984. Statistical properties of single sodium channels. *J. Gen. Physiol.* 84:505–534.

Horn, R., C. Vandenberg, and K. Lange. 1984. Statistical analyses of single sodium channels: effects of *N*-bromoacetamide. *Biophys. J.* 45:323–336.

Josephson, I. R., J. Sanchez-Chapula, and A. M. Brown. 1984. A comparison of calcium currents in rat and guinea pigs single ventricular cells. *Circ. Res.* 54:144–156.

Knopp, K. 1956. Infinite Sequences and Series. Dover Publications, New York. 186 pp.

Lux, H. D., and A. M. Brown. 1984. Patch and whole cell currents recorded simultaneously in small neurons. *J. Gen. Physiol.* 83:727–750.

Mark, G. E., and F. F. Strasser. 1966. Pacemaker activity and mitosis in cultures of newborn rat heart ventricular cells. *Exp. Cell Res.* 44:217–233.

Marty, A., and E. Neher. 1983. Tight seal whole cell recording. *In* Single-Channel Recording. B. Sakmann and E. Neher, editors. Plenum Press, New York. 107–121.

Matteson, P. R., and C. M. Armstrong. 1982. Evidence for a population of sleepy sodium channels in squid axon at low temperatures. *J. Gen. Physiol.* 79:739–758.

Meyer, S. T. 1975. Data Analysis for Scientists and Engineers. John Wiley & Sons Inc., New York. 513 pp.

Nagy, K., T. Kiss, and D. Hoff. 1983. Single Na channels in mouse neuroblastoma cell membrane: indications for two open states. *Pflügers Arch. Eur. J. Physiol.* 399:302–308.

Nelder, J. A., and R. Mead. 1965. A simplex method for function minimization. *Comput. J.* 7:308–313.

Patlak, J. 1984. Two components of single sodium channel inactivation in patch recordings from dissociated cardiac cells. *Biophys. J.* 4:185*a*. (Abstr.)

Patlak, J., and R. Horn. 1982. Effect of *N*-bromoacetamide on single sodium channel currents in excised membrane patches. *J. Gen. Physiol.* 79:333–352.

Patlak, J. B. and M. Ortiz. 1985. Slow currents through single sodium channels of the adult rat heart. *J. Gen. Physiol.* 86:89–104.

Sigworth, F. J., and E. Neher. 1980. Single Na^+ channel currents observed in cultured rat muscle cells. *Nature (Lond.).* 287:447–449.

Ten Eick, R., J. Yeh, and N. Matsuki. 1984. Two types of voltage dependent Na channels suggested by differential sensitivity of single channels to tetrodotoxin. *Biophys. J.* 45:70–73.

Vandenberg, C. A., and R. Horn. 1984. Inactivation viewed through single sodium channels. *J. Gen. Physiol.* 84:535–565.

Wilson, D. L., and A. M. Brown. 1985. Effect of limited interval resolution on single channel measurements with application to Ca channels. *IEEE Trans. Biomed. Eng.* In press.

Yamamoto, D., J. Z. Yeh, and T. Narahashi. 1983. Current-voltage relationships of single sodium channels in neuroblastoma cells. *Biophys. J.* 41:51*a*. (Abstr.)

Zilberter, Y. I., E. N. Timin, Z. A. Bendukidze, and N. A. Burnashev. 1982. Patch-voltage-clamp method for measuring fast inward current in single rat heart muscle cells. *Pflügers Arch. Eur. J. Physiol.* 394:150–155.